Marika Bogdani,[1] Pamela Y. Johnson,[1] Susan Potter-Perigo,[1] Nadine Nagy,[1] Anthony J. Day,[2] Paul L. Bollyky,[3] and Thomas N. Wight[1]

Hyaluronan and Hyaluronan-Binding Proteins Accumulate in Both Human Type 1 Diabetic Islets and Lymphoid Tissues and Associate With Inflammatory Cells in Insulitis

Diabetes 2014;63:2727–2743 | DOI: 10.2337/db13-1658

Hyaluronan (HA) is an extracellular matrix glycosaminoglycan that is present in pancreatic islets, but little is known about its involvement in the development of human type 1 diabetes (T1D). We have evaluated whether pancreatic islets and lymphoid tissues of T1D and nondiabetic organ donors differ in the amount and distribution of HA and HA-binding proteins (hyaladherins), such as inter-α-inhibitor (IαI), versican, and tumor necrosis factor–stimulated gene-6 (TSG-6). HA was dramatically increased both within the islet and outside the islet endocrine cells, juxtaposed to islet microvessels in T1D. In addition, HA was prominent surrounding immune cells in areas of insulitis. IαI and versican were present in HA-rich areas of islets, and both molecules accumulated in diabetic islets and regions exhibiting insulitis. TSG-6 was observed within the islet endocrine cells and in inflammatory infiltrates. These patterns were only observed in tissues from younger donors with disease duration of <10 years. Furthermore, HA and IαI amassed in follicular germinal centers and in T-cell areas in lymph nodes and spleens in T1D patients compared with control subjects. Our observations highlight potential roles for HA and hyaladherins in the pathogenesis of diabetes.

Type 1 diabetes (T1D) is characterized by progressive, immune cell–mediated destruction of pancreatic β-cells that has been partly attributed to a permissive inflammatory milieu (1,2). Although the nature of that inflammatory milieu remains poorly defined, the substrate within which β-cells and migratory inflammatory cells interact is the extracellular matrix (ECM).

The islet ECM is known to make decisive contributions to insulin production, β-cell homeostasis, and proliferation (3–9). However, the nature of the ECM in human T1D and insulitis is poorly understood. In the NOD mouse model of autoimmune diabetes, autoimmune insulitis is associated with remodeling or destruction of basement membranes and the ECM surrounding and/or within islets (7,9–12). This destruction has been proposed as important to the progression to diabetes through the loss of protection from oxidative damage (11) or loss of ECM interactions that make critical contributions to β-cell survival and expansion (3–9).

We have proposed that hyaluronan (HA), a long-chain polysaccharide prominent in inflamed tissues, is a keystone molecule in the inflammatory milieu (6) and is at the center of a complex network of ECM molecules that together exert decisive effects on the physical and immunologic properties of inflamed tissues. This network includes HA-binding molecules called hyaladherins, such as inter-α-inhibitor (IαI), versican, and tumor necrosis factor–stimulated gene-6 (TSG-6) (13). These proteins

[1]Matrix Biology Program, Benaroya Research Institute, Seattle, WA
[2]Wellcome Trust Centre for Cell-Matrix Research, Faculty of Life Sciences, University of Manchester, Manchester, U.K.
[3]Division of Infectious Diseases, Stanford University Medical Center, Stanford, CA
Corresponding author: Thomas N. Wight, twight@benaroyaresearch.org.

Received 1 November 2013 and accepted 24 March 2014.

This article contains Supplementary Data online at http://diabetes.diabetesjournals.org/lookup/suppl/doi:10.2337/db13-1658/-/DC1.

are believed to interact with HA in such a way as to promote the formation of macromolecular complexes that modulate leukocyte adhesion and activation, thus influencing the inflammatory response (14–16). HA is highly abundant in inflamed tissues, and its synthesis is responsible for many of the physiologic changes associated with inflammation, including edema, vascular permeability changes, and leukocyte egress at sites of injury (14), as well as the maturation of dendritic cells (17), antigen presentation (18,19), and the function and number of regulatory T cells (18,20,21).

The composition of the ECM in human T1D islet tissue and in areas of insulitis matters because the inflammatory milieu is believed to be a driving force in T1D. In the current study, we demonstrate for the first time that HA and hyaladherins increase in islets, pancreatic lymph nodes (PLNs), and spleens of younger donors and accumulate in regions of lymphocytic infiltrates in T1D and that both the amount and the distribution of HA and hyaladherins vary with time since diabetes onset. These observations coupled with our recent in vitro studies demonstrating that HA controls T-cell movement (22) and phenotype (20,21) implicate these specific ECM components in the pathogenesis of T1D. Such observations point to a previously unrecognized characteristic of tissues involved in the pathogenesis of T1D and highlight the potential for new targets in the treatment of this disease.

RESEARCH DESIGN AND METHODS

Donors and Tissue Procurement

Pancreas, spleen, and lymph node tissue sections were obtained through the JDRF-sponsored Network for Pancreatic Organ Donors with Diabetes (nPOD) program. Case numbers throughout this article were assigned by nPOD, unless otherwise noted. Tissues were from 13 T1D donors with a diabetes duration of 8 weeks–9 years (younger donors), 4 donors with T1D for 28–66 years (older donors), and 17 age-matched healthy donors. Sections from two pancreatic tissue samples (H1204 and H911) collected at T1D onset were provided by Gun Frisk (University of Uppsala, Uppsala, Sweden). Clinical characteristics of donors are shown in Supplementary Table 1. Sections from one or two pancreas pieces from the body and tail regions, from one spleen piece, or from one to four PLN tissue samples were analyzed for each donor. Spleen sections were available from 11 younger T1D and 15 age-matched healthy donors. PLNs were available from 8 younger T1D and 10 age-matched healthy donors. To evaluate whether changes in the amount of HA occur in other tissues, we examined sections from thymus and duodenum, the only additional organs available at nPOD. Thymus and duodenum sections were available from three younger T1D and four age-matched healthy donors and from seven younger T1D and seven age-matched healthy donors, respectively. All tissues showed well-preserved morphology without any evidence of autolysis. This study was carried out with the approval of the Institutional Review Board of the Benaroya Research Institute.

Histochemistry and Immunohistochemistry

Sections were stained for HA using a biotinylated HA-binding protein (b-HABP) prepared from cartilage and for immunohistochemistry as described (23). In control experiments, slides were predigested with HA-specific *Streptomyces* hyaluronidase, which abolished staining with b-HABP (Supplementary Fig. 1). Antibodies to human CD3, CD20, CD31, and CD45 (all from Abcam, Cambridge, MA) were used at concentrations of 10.0, 1.8, 3.5, 5.0 μg/mL, respectively. Antibodies to synaptophysin (Dako, Carpinteria, CA) and insulin (ab6995; Abcam) were used at dilutions 1:100 and 1:12,000, respectively. Antibodies to glucagon, somatostatin, pancreatic polypeptide (Abcam), TSG-6, and IαI (24,25) were used at a dilution of 1:1,000. The secondary antibodies Alexa Fluor 488– or Alexa Fluor 555–conjugated IgG (Molecular Probes, Grand Island, NY) and peroxidase-labeled IgG were used at 3 μg/mL and 1:200 in PBS, respectively. The nuclei were visualized with DAPI (Sigma-Aldrich, St. Louis, MO). Positive and negative controls were included in each staining experiment. Tissues were examined using a Leica DM IRB microscope, and images were acquired using a Spot Xplorer camera and imaging software. All the images were taken under the same experimental settings and light exposure.

Evaluation of Islet Cell Composition

To evaluate the relative proportion of the classical hormone-producing cells in the endocrine pancreas, consecutive pancreas sections were costained with a rabbit polyclonal antisynaptophysin antibody and a mouse monoclonal antibody against either insulin, glucagon, somatostatin, or pancreatic polypeptide. The number of synaptophysin-positive cells and the number of cells costained for synaptophysin and one of the islet hormones were counted and the relative proportion of costained cells calculated. At least 3,000 cells were counted per pancreas section.

Morphometric Analysis and Quantitation

Whole-section imaging was performed using a NanoZoomer Digital Pathology slide scanner (Hamamatsu; Bridgewater, NJ) at the University of Washington Histology and Imaging Core in Seattle, WA. Slides were scanned in bright-field at a 20× objective and the digital images imported for analysis using Visiopharm software (Hoersholm, Denmark), which provides automated quantification of stained areas and uniform systematic random sampling on whole-section bright-field images (26). The software labeled the marker (HA, IαI, versican, and TSG-6)-positive area vs. tissue area using a project-specific configuration based on a threshold of pixel values. The relative and total tissue areas stained by the markers were measured. All the images were processed together using this configuration to generate the desired outputs (stained and unstained tissue areas measured in square micrometers).

Measurement of Insulin-Positive Areas

Sections were stained for insulin and counterstained with hematoxylin. Using Visiopharm, regions of interest (ROIs) were detected throughout the tissue. The software labeled the insulin-positive (IP) staining and the exocrine pancreas tissue using a project-specific configuration based on a threshold of pixel values. The analysis was run in two steps: *1*) Areas of IP staining were outlined as individual islet profile ROIs, and *2*) the analysis was run within these ROIs to label the IP area within each islet. The images were processed in batches and sampled at 100%.

Quantitation of HA and Hyaladherin-Positive Areas

Pancreatic Islets. Islets were identified by their staining for the panendocrine marker synaptophysin. Thirty percent of the normal islets were sampled according to systematic uniform random sampling (27). The coefficient of variation at 30% sampling of the normal islets was <5%. All diabetic islets present in the tissue sections were analyzed. To better characterize HA and hyaladherin localization in relationship with the peri-islet capillaries, the stained areas were defined as intraislet and peri-islet and are schematically represented in Supplementary Fig. 2. Separating the islets from the exocrine tissue (28–30), the peri-islet capillaries have an islet endocrine cell side and an exocrine cell side. The intraislet area is defined as the area occupied by the islet endocrine cells and bordered by the endocrine side of the peri-islet capillaries. Because the diameter of peri-islet capillaries in normal pancreatic islets has been reported to be on average 4.29 μm (31), the peri-islet area was defined as the area around the islets at a 5-μm distance from the endocrine side of the peri-islet capillaries. The outer border of this area was delineated using the Visiopharm annotation tool. The stained areas were measured using Visiopharm software.

Spleen and PLNs. The B-cell follicles and T-cell areas (32,33) were identified by hematoxylin counterstaining of spleen and PLN sections stained for HA or any of the hyaladherins. To confirm the presence of the B-cell follicles and T-cell areas, consecutive sections were stained immunohistochemically for CD20 and CD3, which label the B and T cells, respectively (Supplementary Fig. 3*A*–*H*). The number of all B-cell follicles, with or without a germinal center (GC), was counted visually, and the proportion of those with a GC was calculated. The follicular GCs were examined for the presence of HA, IαI, TSG-6, and versican staining, and the proportion of GCs that were stained for any of these individual molecules was determined. The areas of follicular GCs and T-cell regions were measured using Visiopharm software (Supplementary Fig. 3*I* and *J*). The HA-, IαI-, TSG-6–, and versican-positive areas within the GCs and T-cell regions were measured, and their relative proportion calculated.

Exocrine Pancreas, Thymus, and Duodenum. The relative HA-positive areas in exocrine pancreas, thymus, and duodenum tissues were measured with Visiopharm. Tissue areas were sampled at 100%.

Evaluation of Insulitis

To detect inflammatory cells, sections were stained for the leukocyte common antigen CD45, a marker of both lymphoid and myeloid cells present in human insulitis after T1D onset (34). Islets were identified with the panendocrine cell marker synaptophysin. No CD45-positive cells were observed in contact with either single endocrine cells or the smallest clusters of fewer than five endocrine cells. These small clusters were not included in subsequent calculations. Islets comprising six or more endocrine cells were counted along with the number of CD45-positive cells in contact with the endocrine cells. Insulitis was evaluated by determining *1*) the percentage of islets with CD45-positive cells adjacent to endocrine cells, and *2*) the number per islet of CD45-positive cells in contact with endocrine cells (Supplementary Fig. 4). There were 0.1 ± 0.1 and 1.8 ± 3.9 CD45-positive cells per islet in normal and diabetic tissues, respectively ($P < 0.0001$). A total of 2,030 normal and 930 diabetic islets from 17 healthy and 19 T1D donors were analyzed.

Statistical Analysis

Data are expressed as mean ± SD of n independent measurements. Significance of the difference between two or more groups of data were evaluated using the Mann-Whitney U or Kruskal-Wallis tests, respectively. Correlation analysis was performed using the nonparametric Spearman rank correlation test. The significance of the difference between two correlation coefficients was assessed using the Fisher test. $P < 0.05$ was considered statistically significant.

RESULTS

HA Accumulates in Human Diabetic Islets

HA was detected around the periphery of normal human islets in a discontinuous pattern and sparsely distributed within the islets (Fig. 1*A* and *B*). Colabeling HA with synaptophysin or CD31 and vimentin revealed that HA located extracellularly, juxtaposed to the islet microvessels (Fig. 1*C* and *D*, Supplementary Figs. 5*A* and *B* and 6*A*–*E*). In diabetic islets, HA occurred similarly outside the endocrine cells in close association with peri- and intraislet capillaries (Fig. 1*E*–*H*, Supplementary Figs. 5*C* and *D* and 6*F*–*I*). However, its abundance, which in normal islets was low and did not change significantly with age, was markedly increased in diabetic islets. Quantification of 794 normal and 775 diabetic islets indicated a 5.2-fold increase in the HA-stained area in diabetic islets (Fig. 1*I*).

HA Accumulates Preferentially in Islets of Younger Diabetic Donors With Shorter T1D Duration

When diabetic islets were examined according to disease duration and compared with the age-matched controls, a significantly higher mean islet HA-positive area was found in tissues of younger donors with diabetes for <10 years but not in those of older donors with long-standing diabetes (Fig. 2*A* and *B*). To determine whether HA accumulation occurred differentially along the islet microvasculature,

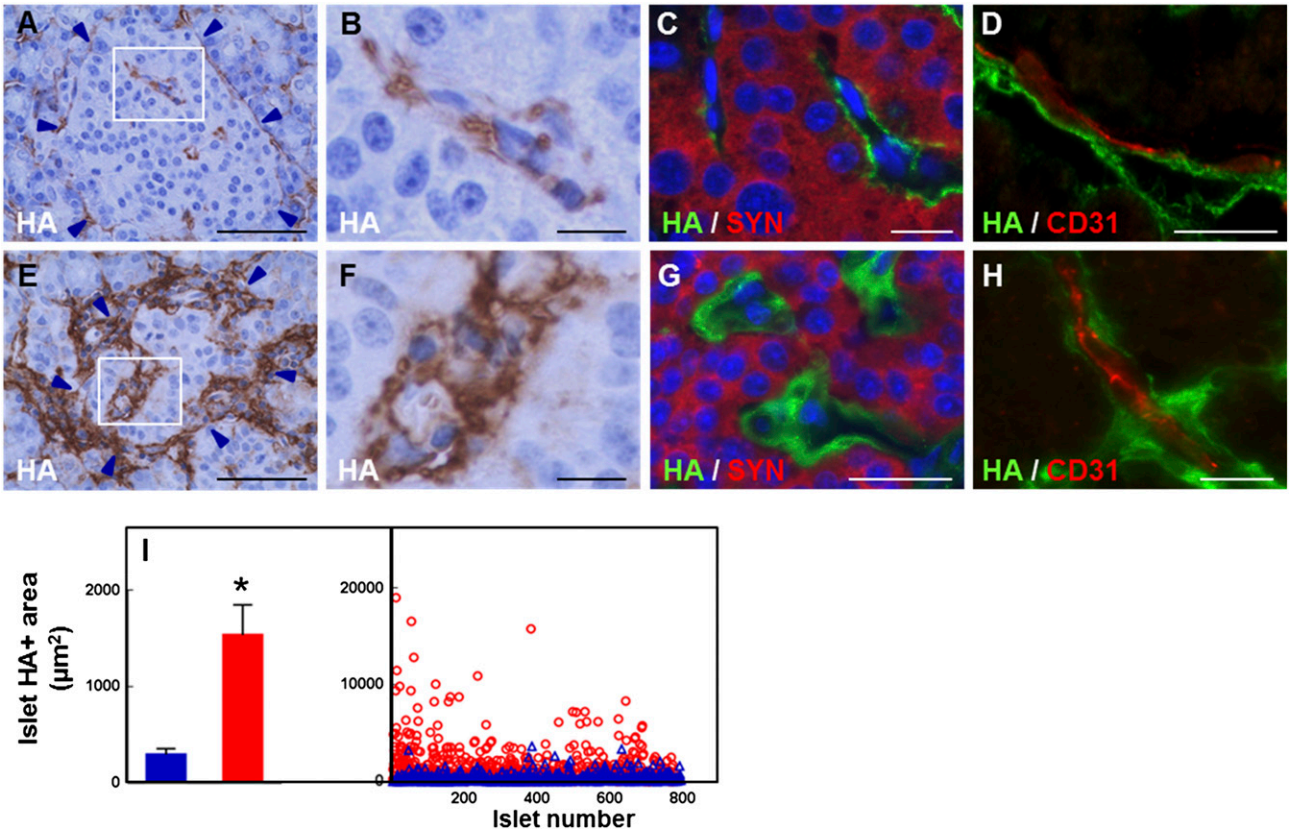

Figure 1—HA accumulation along the microvasculature of human islets in T1D. *A–D*: Images of normal human islets prepared from nPOD case 6153. *A*: Histochemistry shows HA (brown) located around and within the islet. *B*: Higher magnification of the boxed area in *A*. *C*: Colabeling of HA (green) with the panendocrine marker synaptophysin (red) shows HA outside the endocrine cells. *D*: Colabeling of HA (green) with the endothelial cell marker CD31 (red) reveals HA juxtaposed to the islet microvessels. *E–H*: Images of human diabetic islets prepared from nPOD case 6052. *E*: Histochemistry shows abundant HA (brown) located around and within the islet. *F*: Higher magnification of the boxed area in *E*. *G*: Colabeling of HA (green) with synaptophysin (red) reveals abundant HA located outside the endocrine cells. *H*: Colabeling of HA (green) with CD31 (red) shows HA accumulated along the islet microvessels. Arrowheads in *A* and *E* point to the islet border. Scale bar: 50 μm (*A* and *E*) and 10 μm (*B–D* and *F–H*). See also Supplementary Figs. 5 and 6. *I*: Morphometric quantitation of HA in pancreatic islets. Blue bar and △, normal tissues; red bar and ○, diabetic tissues. Mean values (bar graph, mean ± SD) and individual measurements (scatter plot) of the HA staining area of 794 normal and 775 diabetic islets analyzed in tissues of 17 healthy and 19 T1D donors. Each dot in the scatter plot represents the measurement obtained from a single islet. *$P < 0.0001$ vs. normal islets.

the HA staining pattern was quantitated as peri- and intraislet staining (Fig. 2*C–F*). For peri-islet staining, HA was consistently associated with the peripheral capillaries of normal and diabetic islets. Plots of individual measurements of peri-islet HA-positive areas (Fig. 2*C*) and their mean values for each diabetic and control donor (Fig. 2*D*) show heterogeneity in peri-islet HA positivity among the diabetic islets and between the diabetic donors. When compared with the age-matched controls, only the younger diabetic islets contained a significantly larger (6.6-fold) peri-islet HA-stained area. These data indicate that HA accumulated around the edge capillaries of diabetic islets, the site where inflammatory cell infiltrates in insulitis are mostly observed. For intraislet staining, HA was present within a significantly larger proportion of younger diabetic islets than in control islets (99 ± 2% vs. 65 ± 2%, $P < 0.0001$). As with the peri-islet HA, intraislet HA accumulated unequally among the islets. When individual measurements of intraislet HA-positive areas in diabetic islets were compared with those obtained from control islets, their median value was found to be significantly higher (309 vs. 25 μm^2, $P < 0.0001$) (Fig. 2*E*). The intraislet HA-stained area was consistently larger in the diabetic tissues of younger donors compared with control donors (Fig. 2*F*). To assess whether intraislet HA abundance was determined by islet size, we examined the relationship between the intraislet HA positivity and islet area. Histograms of intraislet HA-positive areas and islet areas indicated that more HA was present in larger islets (Fig. 2*G*). However, when the intraislet HA areas were plotted against the islet areas, the correlation coefficient was lower for the diabetic tissues than the control tissues ($P < 0.0001$) (Fig. 2*H*). In addition, the younger diabetic islets showed a 5.9-fold larger intraislet HA-positive area, but only a 1.4-fold higher mean profile area than the control islets (6,677 vs. 4,916 μm^2, respectively). This greater increase in HA positivity compared with the islet area led to a larger relative intraislet HA staining area (Fig. 2*I*).

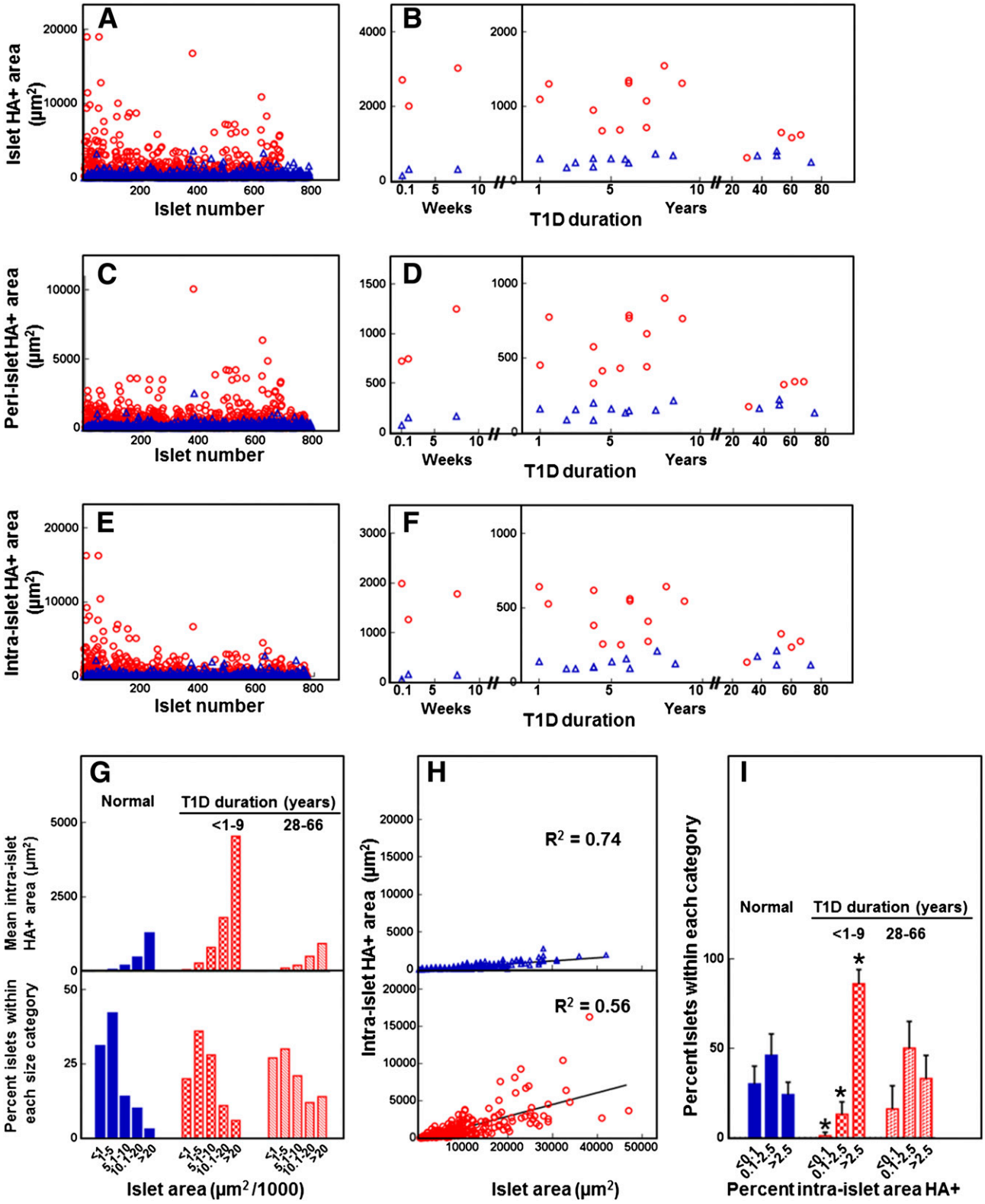

Figure 2—Quantitative analysis of the HA-positive area in human pancreatic islets. Blue bars and △, normal tissues; red bars and ○, diabetic tissues. Analysis included 794 normal and 775 diabetic islets in tissues of 17 healthy donors and 19 T1D donors with diabetes for ≤9 years (n = 15) and ≥28 years (n = 4). *A* and *B*: Morphometric quantification of the islet HA-positive area showing individual measurements obtained from each islet (*A*) and mean values for each individual donor (*B*). *C* and *D*: Morphometric quantification of the peri-islet HA-positive area showing individual measurements obtained from each islet (*C*) and mean values for each individual donor (*D*). *E* and *F*: Morphometric quantification of the intraislet HA-positive area showing individual measurements obtained from each islet (*E*) and mean values for each individual donor (*F*). *G*: Mean intraislet HA-positive area (*top*) measured in the islets falling within each islet area

These data indicate that although the amount of intraislet HA is influenced by the islet mass, the islet size alone is not sufficient to explain the extent to which HA accumulates in younger diabetic islets.

A comparison with the younger age-group showed that in older T1D donors with long-standing diabetes (28–66 years) the islet HA-positive area was significantly less than that of younger diabetic donors and comparable to that observed in both younger and age-matched control donors (Fig. 2*B, D, F, G,* and *I*). The HA staining intensity in the older diabetic tissues was also similar to that observed in the age-matched control tissues. The presence of HA at normal tissue levels in the islets of older T1D donors may have resulted from subsequent clearance of islet HA accumulated previously in the early stages of diabetes development. Alternatively, HA turnover in these islets may have not been altered during the course of the disease.

HA Accumulation in IP and Insulin-Negative Islets of Younger Diabetic Donors

We further examined how HA accumulation in diabetic islets associated with the size of the β-cell population. The relative proportion of IP cells and the relative IP cell areas, although heterogeneous among the individual samples, significantly decreased in the diabetic tissues compared with control tissues (Fig. 3*A–E*, Supplementary Fig. 7*A*). The presence of IP cells also varied among the diabetic tissues. Islets with IP cells were identified in the pancreatic tissues of the three patients who died at disease onset or 8 weeks after and of four T1D patients with disease duration of 1–7 years (Fig. 3*F* and *G*, *top panels*). In these IP tissues, 46 ± 29% of the islets contained IP cells, which accounted for 15 ± 7% of all endocrine cells and 28 ± 13% of the IP islet cells. Both IP and insulin-negative (IN) islets showed larger HA-positive areas than the control islets (Fig. 3*F*, *bottom panel*, Supplementary Fig. 7*B*). Compared with the IN tissues, a significantly larger area of intraislet HA positivity was observed in the IP tissues in which the islet IP area was decreased to 15% of that of control tissues (455 ± 129 vs. 3,032 ± 1,067 μm^2, respectively) (Fig. 3*G*, *bottom panels*). Within the IP tissues, the largest intraislet HA-positive areas were observed in diabetic tissues collected within 1 year of disease onset in which the IP cell areas were decreased to 26% of the control tissues (797 ± 83 vs. 3,032 ± 1,067 μm^2) (Fig. 3*G*, green arrows). The data indicate that although HA accumulation is a feature of tissues of younger diabetic donors, the largest HA depositions are observed in the IP tissues, particularly those collected within 1 year of disease onset and which had undergone a partial loss of β-cells. The presence of increased HA amounts in IN islets, although in amounts significantly lower than those in the IP islets, suggests that HA accumulation precedes β-cell loss.

HA Amasses in Sites of Islet Inflammation

In addition to accumulating around and inside the islets, HA also amassed within the clusters of leukocytes in regions exhibiting insulitis (Fig. 4*A* and *B*). Dispersed or aggregated CD45-positive cells infiltrated the islets or gathered at their periphery adjacent to the endocrine cells (Fig. 4*C* and *D*, Supplementary Fig. 4). These CD45-positive cells were consistently observed surrounded by and embedded in a meshwork of HA (Fig. 4*C* and *D*). The proportion of islets with CD45-positive cells in the younger diabetic tissues, although variable, was significantly higher than in control tissues and associated with HA accumulation (Fig. 4*E* and *F*). The extent of inflammatory cell infiltrates and the abundance of HA in islets of older diabetic donors were comparable to the age-matched control donors (Figs. 2 and 4*E* and *F*).

Hyaladherins Are Present in Human Islets and Associate With Inflammatory Cells in Insulitis

To determine whether changes also occurred in the ECM proteins that bind and interact with HA, we evaluated the IαI, versican, and TSG-6 patterns in diabetic and control islets. IαI was detected around the periphery of normal (Fig. 5*A* and *B*) and diabetic (Fig. 5*C* and *D*) human islets and inside the islets in a pattern consistently similar to that observed with HA (Fig. 5*E–H*). In normal islets, IαI staining was sparse and of moderate intensity regardless of donor age. In contrast, IαI was abundant in diabetic islets, with a 4.8- and 5.1-fold higher IαI-positive area around and within the islets, respectively, compared with control islets (Fig. 5*I*). In diabetic tissues, IαI staining was more intense than in control tissues. As with HA, IαI accumulation was a characteristic of islets of younger T1D donors in which the relative IαI-positive area increased 8.1-fold versus the age-matched control donors ($P < 0.0001$) (Fig. 5*J–L*). IαI also accumulated in the insulitis areas where aggregates of inflammatory cells were observed enclosed in an IαI meshwork (Fig. 5*M*). In islets of long-standing diabetic donors, the IαI abundance was low and comparable to that observed in the age-matched control donors (Fig. 5*J–L*).

Versican was barely detectable in the normal islets, but when present, it was associated with the islet microvessels (Fig. 5*N* and *O*) within the HA- and IαI-rich areas. A similar localization pattern of versican was observed in the diabetic islets (Fig. 5*P* and *Q*). Although its overall abundance was low, the relative versican-positive area was sixfold higher in the younger diabetic islets (Fig. 5*R*),

category (*bottom*). *H*: Individual measurements of intraislet HA-positive areas plotted as a function of islet area. Spearman correlation coefficients are shown. *I*: Percent intraislet HA-positive area in normal and diabetic pancreata. *$P < 0.0001$ vs. normal tissues.

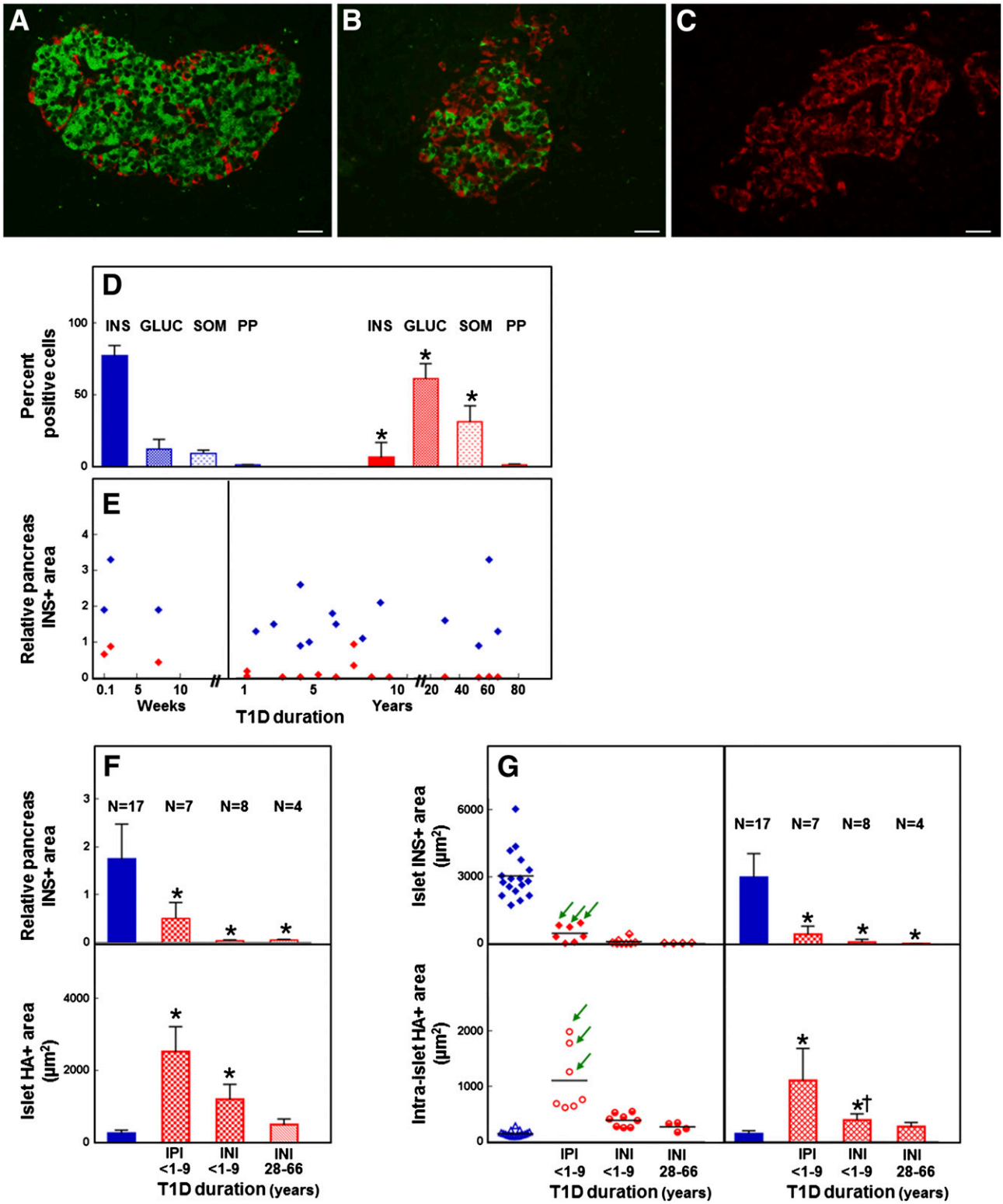

Figure 3—*A–C*: Immunohistochemistry for insulin (green), glucagon, somatostatin, and pancreatic polypeptide (red) of normal (*A*) and diabetic (*B* and *C*) islets. Images were prepared from nPOD cases 6153 (*A* [healthy]), 6052 (*B* [T1D]), and 6064 (*C* [T1D]). Scale bar: 25 µm. *D–G*: Quantitative analysis of the islet cell composition and HA-positive areas in human pancreas. *D*: Relative proportion of the classic pancreatic hormone-producing cells. Blue bars, normal tissues; red bars, diabetic tissues. Data are mean ± SD of measurements obtained from tissues of 17 healthy and 19 T1D donors. *$P < 0.0001$ vs. normal tissues. There was no significant difference in the percentage of pancreatic polypeptide-positive cells between the normal and long-standing diabetic tissues ($P = 0.1464$). *E*: Relative pancreas IP area. Red ◆, diabetic tissues; blue ◆, age-matched normal tissues. Data represent mean values of measurements obtained for each of the 17 healthy and 19 T1D donors. *F*: Relative IP area (*top*) and islet HA-positive area (*bottom*). Blue bars, normal tissues; red bars, diabetic tissues. Data are mean ± SD of measurements obtained from tissues of 17 healthy and 19 T1D donors. The tissues of older diabetic

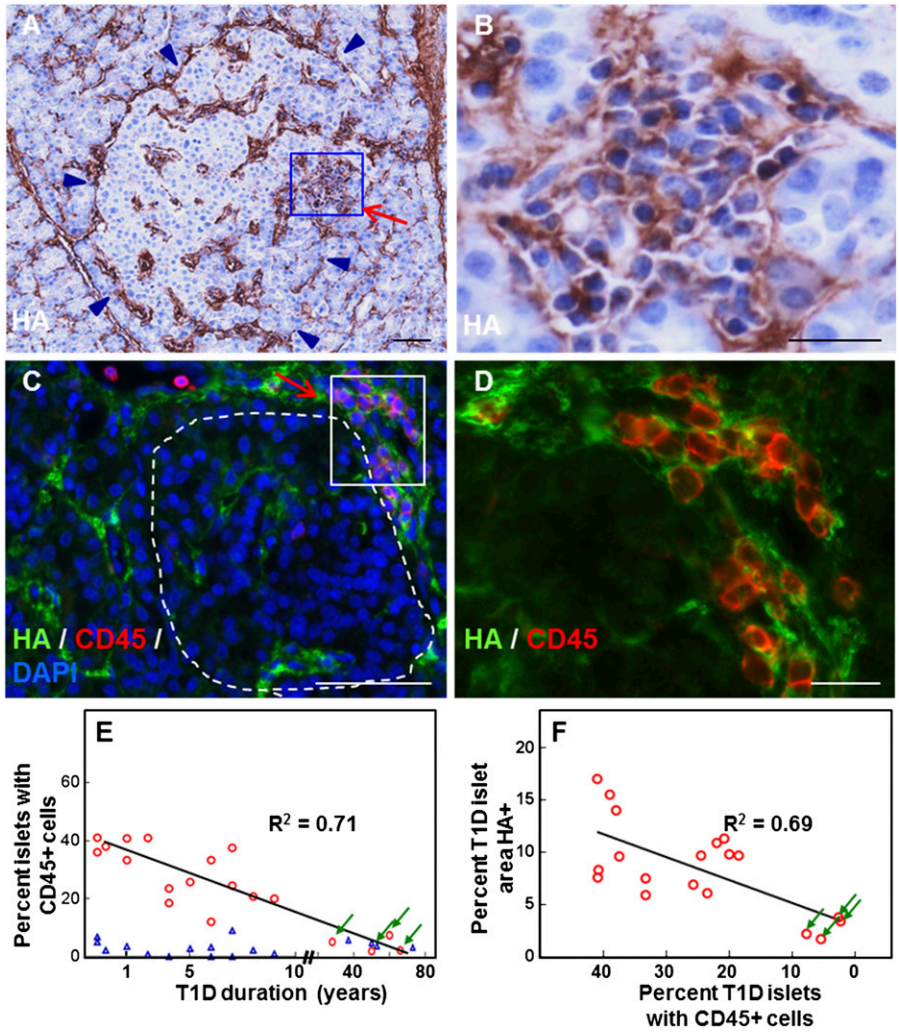

Figure 4—HA accumulation in insulitis in human T1D. *A–D*: Images show two diabetic islets with insulitis: nPOD cases 6052 (*A* and *B*) and 6070 (*C* and *D*). Arrows point to insulitis areas (*A* and *C*). *A*: Histochemistry reveals HA (brown) in the islet and insulitis area. Arrowheads point to the islet border. *B*: Higher magnification of the boxed area in *A*. *C*: Colabeling of HA (green) with the leukocyte common antigen CD45 (red) confirms the presence of HA in the sites of inflammatory infiltrate. The islet is delineated with a dashed line. *D*: Higher magnification of the boxed area in *C*. *E*: Scatter plot of the proportion of islets with CD45-positive inflammatory cells as a function of diabetes duration. A total of 2,030 normal and 930 diabetic islets from 17 healthy and 19 T1D donors were analyzed. $P < 0.0001$ vs. normal tissues. ○, diabetic tissues; △, age-matched normal tissues. *F*: Scatter plot of relative HA-stained islet areas as a function of the proportion of CD45-positive islets in diabetic tissues. Arrows point to measurements obtained from tissues of older T1D donors (*E* and *F*). See also Supplementary Fig. 4.

a difference comparable to that observed for HA and IαI. Additionally, similar to HA and IαI, versican was present in the insulitis area and located around the inflammatory cells (Fig. 5*S*). In the tissues of younger diabetic donors, versican staining intensity was stronger than in the control tissues and tissues of older diabetic donors.

In normal tissues, TSG-6 staining occurred in the endocrine cell compartment and did not appear to

donors did not contain IP islets. *$P < 0.0001$ vs. normal tissues. There was no significant difference in the islet HA-positive area between the tissues of older diabetic donors and age-matched normal tissues ($P = 0.2$). *G*: Mean islet IP area (*top*) and HA-positive area measured within these islets (*bottom*). Blue ◆, bars, and △, normal tissues; red ◆, ◇, bars, ○, and ●, diabetic tissues. Data were obtained from tissues of 17 healthy and 19 T1D donors and are mean values for each individual donor (*left panels*) and mean ± SD of individual values in each donor group (*right panels*). Arrows point to tissues collected within 1 year of disease onset. The tissues of older diabetic donors did not contain IP islets. *$P < 0.0001$ vs. normal tissues, †$P = 0.0003$ vs. IP islet tissues. There was no significant difference in the intraislet HA-positive area between the tissues of older diabetic donors and the age-matched normal tissues ($P = 0.2$). GLUC, glucagon; INI, insulin-negative islets; INS, insulin; IPI, IP islets; PP, pancreatic polypeptide; SOM, somatostatin. See also Supplementary Fig. 7.

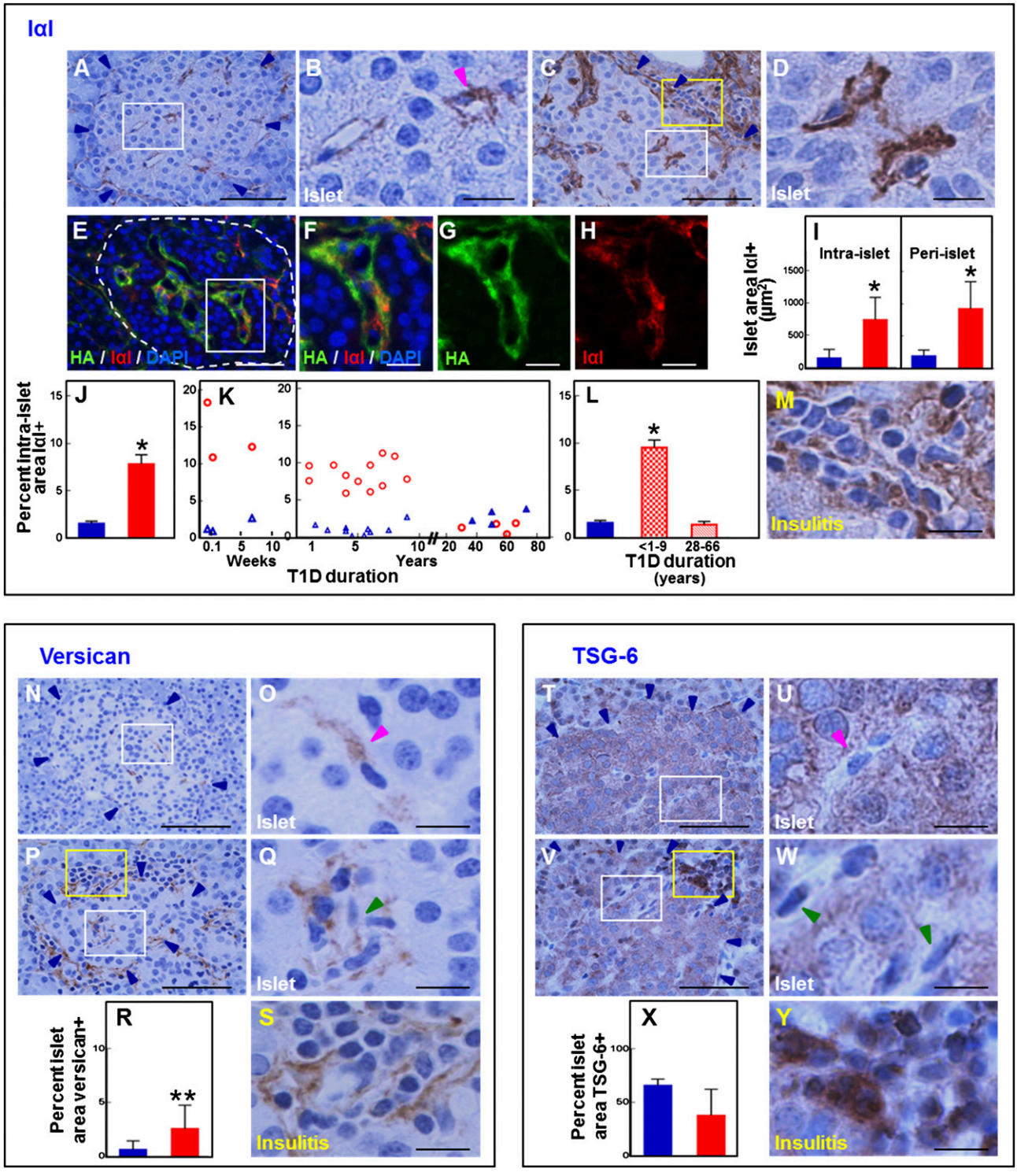

Figure 5—Staining pattern of the HA-binding proteins IαI, versican, and TSG-6 in normal and diabetic islets and insulitis. *A–M*: Immunohistochemistry for IαI and morphometric quantification of the IαI-positive islet area. *A–D*: Immunohistochemistry reveals IαI in normal (*A* and *B*) and diabetic (*C* and *D*) islets. *B* and *D*: Images show higher magnification of the tissue areas within the white boxes in *A* and *C*. Blue arrowheads point to the islet border. The magenta arrowhead points to an intraislet capillary. *E–H*: Colabeling of IαI (red) with HA (green) indicates that IαI occurs in the HA-rich regions along the islet microvessels. Nuclei (blue) are visualized with DAPI. *F–H*: Images show higher magnification of the boxed area in *E*. *I*: Mean ± SD of peri- and intraislet IαI-positive areas obtained from tissues of 17 healthy and 19 T1D donors. *J–L*: Relative IαI-positive islet area showing mean ± SD (*J*) and individual values (*K*) of measurements obtained from tissues of 17 healthy and 19 T1D donors. *L*: Mean ± SD of measurements obtained from tissues of 17 healthy donors and 19 T1D donors with diabetes for ≤9 years (n = 15) and ≥28 years (n = 4). Blue bars and △, normal tissues; red bars and ○, diabetic tissues. *P < 0.0001 vs. normal tissues. *M*: Image shows higher magnification of the tissue area within the yellow box in *C*. Immunohistochemistry reveals IαI accumulation in insulitis. Scale bars: 50 μm (*A*, *C*, and *E*) and 10 μm (*B*, *D*, *F–H*, and *M*). *N–S*: Immunohistochemistry for versican and morphometric quantification of the intraislet versican-positive area. *N*: Immunohistochemistry shows that versican is sparse in normal islets. *O*: Higher

associate with the islet microvasculature (Fig. 5*T* and *U*). The staining was consistently granular throughout the cell cytoplasm and of moderate intensity with little variation among the normal islets. In diabetic tissues, TSG-6 immunoreactivity was also confined to the endocrine compartment (Fig. 5*V* and *W*). TSG-6 staining intensity varied from islet to islet and within the islets in which patches of more intensely stained endocrine cells occurred adjacent to weakly stained islet cells. Although there was a trend toward reduced TSG-6 staining area in diabetic islets, it was of borderline significance ($P = 0.0554$) (Fig. 5*X*). As with IαI and versican, TSG-6 was observed in the insulitis area. However, in contrast to IαI and versican, TSG-6 occurred intracellularly and appeared to intensely stain a subset of inflammatory cells (Fig. 5*Y*). These observations indicate that hyaladherins IαI, versican, and TSG-6 occur in diabetic islets and associate with inflammatory cells in insulitis.

HA Accumulates in Lymphoid Tissues in T1D

Because much of the immune response directed against islet antigens originates in draining lymph nodes and spleen, we sought to ascertain whether there were changes in HA and hyaladherins in lymphoid tissues from T1D and control donors. In normal spleen tissues, HA was sparse and patchy in the B-cell follicular GCs and was not visualized in the B-cell follicular mantle (Fig. 6*A* and *B*). In contrast, HA was abundant in GCs of diabetic spleens, which showed an intense punctate HA staining (Fig. 6*C* and *D*). The fraction of diabetic B-cell follicles with GCs was comparable to that found in the control tissues (Fig. 6*E*). However, a significantly higher proportion of diabetic GCs contained HA, occupying an 8.6-fold larger GC area than in the normal tissues (Fig. 6*E* and *F*).

HA was consistently present in the normal T-cell compartment (Fig. 6*G* and *H*) and exhibited a reticular pattern, appearing to form an HA network along cords of immune cells bordered by the fibroblastic reticular meshwork (35). The T-cell areas were enlarged in diabetic tissues (1.4-fold vs. control tissues) and showed marked accumulation of HA, which appeared as intensely stained large amorphous aggregates (Fig. 6*I* and *J*) that comprised an area 4.7-fold greater than in control tissues (Fig. 6*K*). In both normal and diabetic spleen, HA stained the splenic capsule (not shown) and vessel walls (Fig. 6*C*, *G*, and *I*).

In normal PLNs, HA was sparse and patchy in the normal follicular GCs (Fig. 6*L* and *M*, Supplementary Fig. 8*A*). In adjacent interfollicular regions (IFRs), HA staining displayed a distinct, fine, tram-like pattern that is consistent with localization to the reticular fiber network (Fig. 6*N* and *O*). HA accumulated most strikingly in diabetic PLN GCs and IFRs where the HA staining pattern was more intense and coarser than in normal tissues (Fig. 6*P–S*, Supplementary Fig. 8*B*). HA was observed as numerous small, dense granules distributed over a larger PLN area than in control tissues (Fig. 6*T*). Similar proportions of B-cell follicles in diabetic and normal PLN showed GCs (Fig. 6*U*). However, a greater proportion of diabetic GCs (96% vs. 16% in normal tissues) contained HA that resided in an 89-fold larger area than in control tissues (Fig. 6*U* and *V*). HA stained the normal and diabetic PLN sinuses' wall and the trabecular extensions of the gland fibrotic capsule and formed thin ring-like structures around the capillaries and high endothelial venules (not shown).

Presence of Hyaladherins in Lymphoid Tissues

IαI staining was clearly visible in the GCs of diabetic spleens, whereas IαI immunostaining was barely detectable in the GCs of normal tissues (Fig. 7*A–D*). IαI was also sparse in the T-cell areas of normal spleens and appeared to locate in the HA-rich regions. A small subset of cells in the T-cell compartment stained for IαI and displayed intense IαI cytoplasmic immunoreactivity (Fig. 7*E* and *F*). IαI accumulated in B- and T-cell compartments in diabetic spleens (Fig. 7*G* and *H*). The relative IαI-positive areas in GCs and T-cell regions measured 8.7 ± 1.5% and 9.7 ± 2.3%, respectively, and were significantly larger than those found in the control counterparts (0.3 ± 0.1% and 1.4 ± 0.5%, respectively) (Fig. 7*I*). Intense IαI staining was observed in a subset of immune cells located in the perifollicular region and the splenic red pulp (Fig. 7*A*, *C*, *E,* and *G*).

TSG-6 immunoreactivity was observed in normal and diabetic spleens and occurred intracellularly in lymphoid

magnification of the boxed area in *N*. *P*: Immunohistochemistry shows that versican accumulates in diabetic islets and locates adjacent to the islet microvessels (white box) and in insulitis area (yellow box). *Q* and *S*: Higher magnification of tissue areas within the white and yellow boxes, respectively, in *P*. Blue arrowheads point to the islet border. Magenta and green arrowheads point to intraislet capillaries. Images were prepared from nPOD cases 6153 (healthy) and 6052 (T1D). Scale bar: 50 μm (*N* and *P*) and 10 μm (*O*, *Q*, and *S*). *R*: Morphometric quantification of the relative versican-positive islet area. Blue bar, normal tissues; red bar, diabetic tissues. Data are mean ± SD of measurements obtained from tissues of 17 healthy and 19 T1D donors. $^{**}P = 0.00154$ vs. normal tissues. *T–Y*: Immunohistochemistry for TSG-6 and morphometric quantification of the intraislet TSG-6–positive area. *T*: Immunohistochemistry shows that TSG-6 occurs within the pancreatic endocrine cells in normal tissues. *U*: Higher magnification of the boxed area in *T*. *V*: Immunohistochemistry shows that TSG-6 is present in diabetic islets (white box) and in a subset of inflammatory cells in insulitis (yellow box). *W* and *Y*: Higher magnification of tissue areas within the white and yellow boxes, respectively, in *V*. Blue arrowheads point to the islet border. Magenta and green arrowheads point to intraislet capillaries. Images were prepared from nPOD cases 6153 (healthy) and 6052 (T1D). Scale bar: 50 μm (*T* and *V*) and 10 μm (*U*, *W*, and *Y*). *X*: Morphometric quantification of the relative TSG-6–positive islet area. Blue bar, normal tissues; red bar, diabetic tissues. Data are mean ± SD of measurements obtained from tissues of 17 healthy and 19 T1D donors. There was a trend toward reduced TSG-6 staining area ($P = 0.0554$).

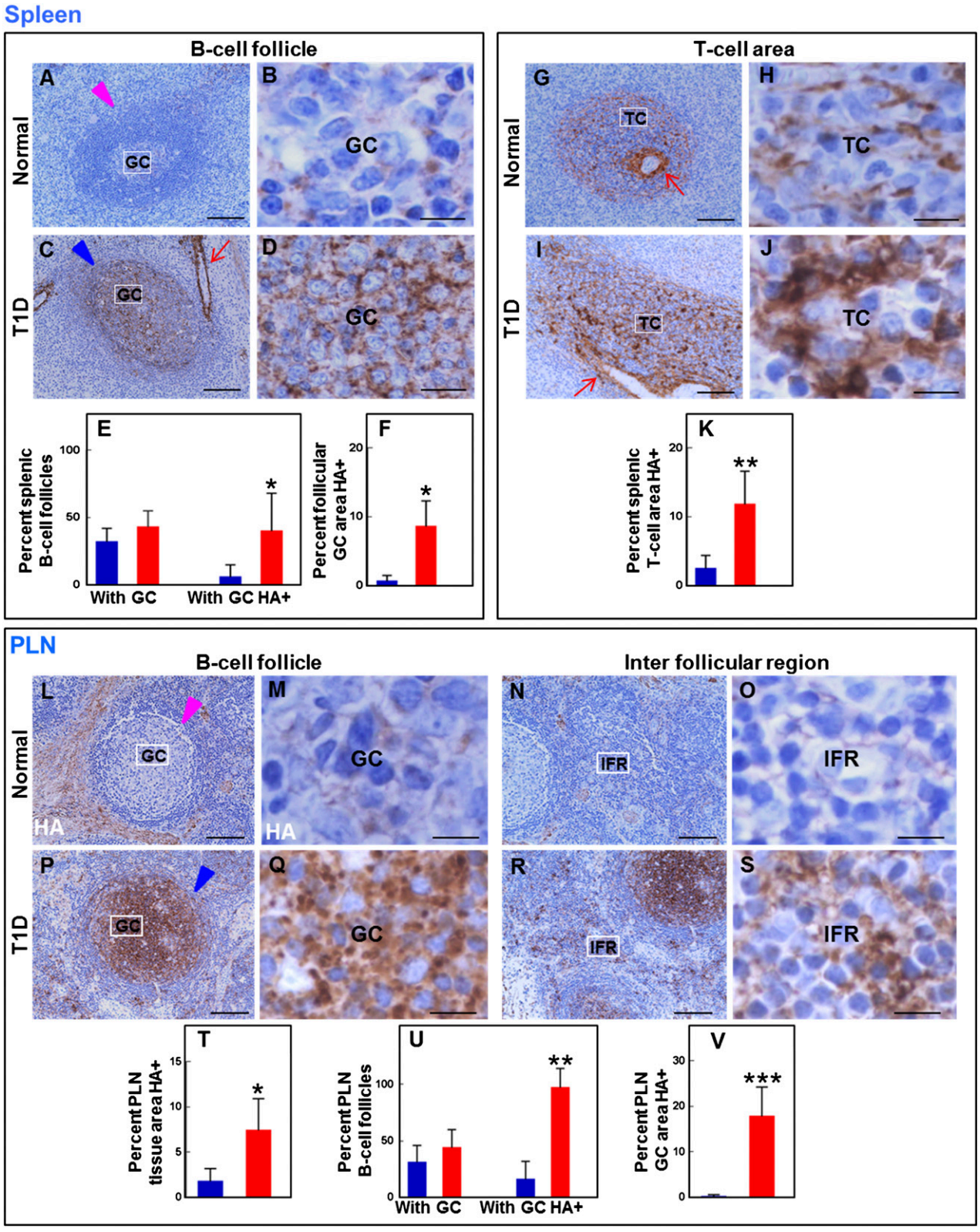

Figure 6—Altered HA distribution and amount in lymphoid tissues in T1D for spleen (*A–K*) and PLNs (*L–V*). *A–F*: Histochemistry for HA and morphometric quantification of the HA-positive area in splenic B-cell follicles. *A*: HA is sparse in follicular GCs in normal tissues. The arrowhead points to a B-cell follicle. *B*: Higher magnification of the boxed area in *A*. *C*: HA is abundant in follicular GCs in diabetic tissues. The arrowhead points to a B-cell follicle; the arrow indicates an HA-positive splenic vessel. *D*: Higher magnification of the boxed area in *C*. Images were prepared from nPOD cases 6196 (healthy) and 6052 (T1D). Scale bars: 100 μm (*A* and *C*) and 10 μm (*B* and *D*). *E* and *F*: Morphometric quantification of the HA-positive area in B-cell follicles. Blue bars, normal tissues; red bars, diabetic tissues. Data are mean ± SD of the measurements of 203 and 236 secondary follicles present in the spleen tissue sections of 15 healthy and 11 T1D donors,

cells. The normal (Fig. 7*J* and *K*) and diabetic (Fig. 7*L* and *M*) follicular GCs showed intense positive TSG-6 staining, whereas the follicular mantle cells in both tissues stained weakly for TSG-6. A subset of lymphoid cells in normal (Fig. 7*N* and *O*) and diabetic (Fig. 7*P* and *Q*) T-cell areas stained moderately positive for TSG-6. Staining pattern and abundance of TSG-6 were not altered in diabetic splenic B- and T-cell compartments (Fig. 7*R*). Similar to IαI, TSG-6 was also observed in a subset of immune cells located in the splenic perifollicular region and red pulp, tissue compartments that were characterized by a lack of HA or versican staining in the immune cells.

In normal PLN, IαI staining was observed around and along the subcapsular and medullary sinuses' vascular walls. It was very sparse in the lymphoid cell compartments (Fig. 7*S* and *T*). Although overall IαI abundance was low, the IαI-positive area was significantly increased in diabetic PLNs compared with control PLNs (Fig. 7*U–W*, Supplementary Fig. 9*A*). Normal PLN also stained for TSG-6, which produced an intense cytoplasmic staining in most cells in B-cell follicles (Fig. 7*X* and *Y*) and in IFRs (data not shown). This staining pattern was not altered in diabetes (Fig. 7*Z*, *Â* and *Ã*). There was a trend toward reduced TSG-6 staining area in diabetic PLNs, but it did not reach significance ($P = 0.0728$) (Fig. 7*Ã*, Supplementary Fig. 9*A*). In normal lymphoid tissues, versican staining was confined to the vascular wall and basement membrane and to a small subset of immune cells in the splenic red pulp. Versican was not visualized in the B- and T-cell areas, and its pattern was not altered in diabetes (Supplementary Fig. 9*B–O*).

No Differences in Relative HA-Positive Area in Other Tissues of T1D Patients Versus Control Subjects

To determine whether HA accumulation occurred in other tissues in T1D, we examined the relative HA-positive area in the exocrine pancreas, thymus, and duodenal mucosa of T1D patients with disease duration of <10 years. No significant differences in HA-positive areas were observed between the T1D and control samples (Supplementary Fig. 10). The data indicate that local accumulation of HA in islets and lymphoid tissue in T1D patients with shorter disease duration is not associated with increased HA deposition in the exocrine pancreas, thymus, and duodenal mucosa.

No Differences in Serum HA Levels in T1D Patients Versus Control Subjects

To determine whether HA accumulation in pancreatic islets and lymphoid tissue was associated with changes in circulating HA, blood samples collected from 20 T1D patients within 1 year of diagnosis and 20 healthy age-matched control subjects were assayed. No significant differences in plasma HA were observed between the T1D and control samples (248 ± 95 and 232 ± 70 ng/mL, $P = 0.9816$). The data indicate that local accumulation of HA in islets and lymphoid tissue in T1D patients with recent disease onset is not associated with increased circulating levels, which have been observed in T1D patients ≥15 years after diagnosis (36).

DISCUSSION

Although the triggering mechanism of T1D is still not clear, the entire process likely relies on the migration of inflammatory cells from the bloodstream into the pancreatic islets through interaction with the ECM that lies between islet capillaries and endocrine cells. However, the nature of islet ECM changes in T1D and how altered ECM and extracellular signals affect disease pathogenesis are poorly understood. Fibrillar ECM components, such as collagens and laminins, have been described as constituents of the human islet capillary basement membrane (7,37,38). In the NOD mouse, disruption of islet capillary basement membrane integrity has been suggested as the initial step in the progression to destructive insulitis (7,9). Disintegration of the laminin-rich capillary basement membrane was also observed in human T1D islets (7). However, it is not known whether loss of the islet capillary basement membrane is the initial event in human insulitis and whether it affects the inflammatory cell phenotype. Others have found major changes in heparan sulfate glycosaminoglycans within human islets during T1D progression (11). Recent studies have identified HA and hyaladherins in the ECM in mouse islets (23), but their involvement in human T1D has not been explored.

respectively. *E*: Prevalence of B-cell follicles with GCs and of follicular GCs containing HA. **P* = 0.0210 vs. normal tissues. *F*: Morphometric quantification of the GC area stained by HA. **P* = 0.0260 vs. normal tissues. *G–K*: Histochemistry for HA and morphometric quantification of the HA-positive area in splenic T-cell (TC) areas. *G*: HA appears to form a network in the TC areas in normal tissues. The arrow points to an HA-positive splenic vessel. *H*: Higher magnification of the boxed area in *G*. *I*: HA is abundant in the TC areas in diabetic tissues. The arrow indicates an HA-positive splenic vessel. *J*: Higher magnification of the boxed area in *I*. Images were prepared from nPOD cases 6196 (healthy) and 6052 (T1D). Scale bars: 100 μm (*G* and *I*) and 10 μm (*H* and *J*). *K*: Morphometric quantification of the HA-positive area. Blue bars, normal tissues; red bars, diabetic tissues. Data are mean ± SD of the measurements obtained from 15 healthy and 11 T1D donors. ***P* < 0.0001 vs. normal tissues. *L–V*: Histochemistry for HA and morphometric quantification of the HA-positive area in PLN. *L–O*: Histochemistry reveals that HA is sparse in B-cell follicles (*L* and *M*) and IFRs in normal tissues (*N* and *O*). *M* and *O*: Higher magnification of the boxed areas in *L* and *N*, respectively. *P–S*: Histochemistry shows HA accumulation in diabetic tissues. *Q* and *S*: Higher magnification of the boxed areas in *P* and *R*, respectively. Images were prepared from nPOD cases 6196 (healthy) and 6052 (T1D). Scale bars: 100 μm (*L*, *N*, *P*, and *R*) and 10 μm (*M*, *O*, *Q*, and *S*). *T–V*: Morphometric quantification of the HA-positive area. Blue bars, normal tissues; red bars, diabetic tissues. Data are mean ± SD of the measurements of 160 and 167 B-cell follicles present in the PLN tissue sections of 10 healthy and 8 T1D donors. **P* = 0.0002, ***P* = 0.0263, ****P* < 0.0001 vs. normal tissues. See also Supplementary Fig. 8.

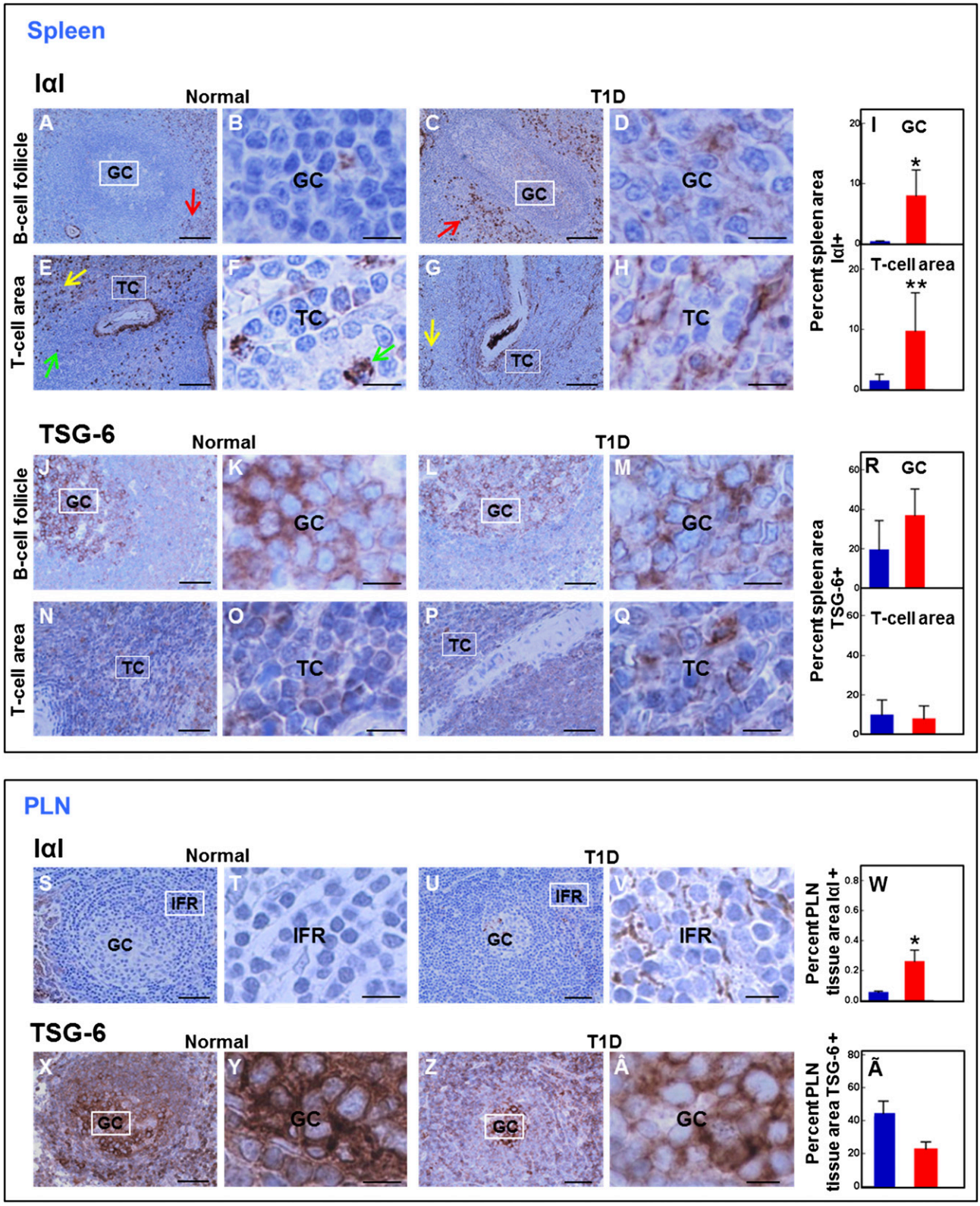

Figure 7—Staining pattern of the hyaladherins, IαI, versican, and TSG-6 in lymphoid tissue for spleen (*A–R*) and PLNs (*S–Ã*). *A–I*: Immunohistochemistry for IαI and morphometric quantification of the IαI-positive area. *A* and *B*: IαI is sparse in follicular GCs in normal tissues. *C* and *D*: IαI is abundant in follicular GCs in diabetic tissues. Red arrows indicate a subset of IαI-positive immune cells in the perifollicular region. *E* and *F*: IαI is sparse in the T-cell (TC) areas in normal tissues. *G* and *H*: IαI is abundant in the TC areas in diabetic tissues. Green arrows point to IαI-positive cells in the TC area. Yellow arrows indicate a subset of IαI-positive immune cells in the red pulp. *B*, *D*, *F*, and *H*: Higher magnification of boxed areas in *A*, *C*, *E*, and *G*, respectively. *I*: Morphometric quantification of the IαI-positive areas in the indicated tissue compartments. Blue bars, normal tissues; red bars, diabetic tissues. Data are mean ± SD of the measurements of 202 and 236 secondary follicles present in the spleen tissue sections of 15 healthy and 11 T1D donors, respectively. **P* = 0.0003, ***P* = 0.0012

The present study has three notable findings. First, HA accumulates in islets from T1D subjects with disease duration of <10 years but not in control subjects. The largest HA depositions were observed in the IP diabetic tissues, particularly those collected within 1 year of disease onset and which had undergone a partial loss of the β-cell population. Moreover, HA accumulation was closely associated with infiltrating lymphocytes. This is strong circumstantial evidence indicating a link among HA deposits, pancreatic β-cell loss, and autoimmune insulitis. Although we are unable to discern whether this link is causative or merely correlative, it has been shown that HA can accelerate the recruitment, proliferation, retention, and activation of leukocytes in other inflamed tissues (16,39–41), and it may be that alterations in HA likewise promote inflammatory responses in T1D. HA is associated with chronic inflammation in other tissues, and in animal models, HA has been implicated in several key events in innate and adaptive immune responses (6,42–44).

The source of HA in islets and insulitis is unclear. In most tissues, mesenchymal cells are prolific producers of HA, made in response to inflammatory mediators. However, both myeloid and lymphoid cells are also capable of synthesizing HA and hyaladherins (18,45), so leukocytes may be a source of this ECM in T1D. In addition, morphologic association of HA with endothelial cells in the islets may be indicative of an endothelial origin because endothelial cells are known to synthesize HA (14). We are actively investigating this question.

Second, we report for the first time that the amount and distribution of hyaladherins, specifically IαI and versican, are increased in human diabetic islets and autoimmune insulitis, whereas TSG-6 is decreased. HA interactions with leukocytes in inflamed tissues are determined by a diverse group of hyaladherins that incorporate HA into cross-linked structures with different architectures and functional activities (15,39,46). Cross-linked HA ECM is capable of interacting with cell surface proteins, proteases, chemokines, and growth factors to affect processes involved in the promotion of leukocyte adhesion, migration, activation, and retention. Under inflammatory conditions, covalent transfer of heavy chains from IαI to HA catalyzed by the protein product of TSG-6 forms the heavy chain–HA complex, a form of HA that promotes the adhesion of leukocytes to HA-rich matrices (15,39,40). Binding of monocytes to HA-rich matrices is also attributed to versican, another proteoglycan that binds HA (47). ECM enriched in HA and versican is synthesized by tissue resident cells in response to inflammatory mediators and influences myeloid and lymphoid cell accumulation in inflamed tissues (15,22,25,39,40,46–48). HA, versican, and IαI are frequently observed together in sites of inflammatory infiltrates, suggesting a causal relationship between their accumulation and leukocyte aggregation (15,39,40). It is conceivable, therefore, that quantitative or qualitative changes in the composition and structure of these HA-rich matrices would alter the tissue microenvironment and affect its function during the course of an inflammatory response.

Further, we found that TSG-6 is present within islet endocrine cells and in inflammatory cells in human insulitis. This is consistent with our findings in mouse pancreatic endocrine cells (23) and those reported in studies of NOD mice (12). A recent study demonstrated that TSG-6 delays the onset of spontaneous autoimmune diabetes in NOD mice by inhibiting insulitis and augmenting regulatory T cells within the pancreas (49). This study further showed that multiple treatments of TSG-6 rendered antigen-presenting cells more tolerogenic, capable of enhancing the generation of regulator T cells, and delayed diabetes in an adoptive transfer model, suggesting that TSG-6 may have immunomodulatory properties. The finding of intracellular localization of TSG-6 suggests that this protein may also be involved in other cellular functions and may be protective to pancreatic β-cells. In neutrophils and mast cells, TSG-6 is stored in secretory granules and released in response to proinflammatory signals (50,51). Because islet endocrine cells contain secretory granules that store peptide hormones for subsequent

vs. normal tissues. *J–R*: Immunohistochemistry for TSG-6 and morphometric quantification of the TSG-6–positive area. *J–M*: TSG-6 staining is present in follicular GCs in normal (*J* and *K*) and T1D (*L* and *M*) tissues. *N–Q*: TSG-6 staining is present in a subset of immune cells in the TC areas in normal (*N* and *O*) and diabetic (*P* and *Q*) tissues. *K*, *M*, *O*, and *Q*: Higher magnification of the boxed areas in *J*, *L*, *N*, and *P*, respectively. *R*: Morphometric quantification of the TSG-6–positive area in the indicated tissue compartments. Blue bars, normal tissues; red bars, diabetic tissues. Data are mean ± SD of the measurements of 203 and 236 secondary follicles present in the spleen tissue sections of 15 healthy and 11 T1D donors, respectively. TSG-6–stained areas in normal and diabetic follicular GC ($P = 0.9090$) or TC areas ($P = 0.5481$) were similar. Images were prepared from nPOD cases 6196 (healthy) and 6052 (T1D). Scale bars: 100 μm (*A*, *C*, *E*, *G*, *J*, *L*, *N*, and *P*) and 10 μm (*B*, *D*, *F*, *H*, *K*, *M*, *O*, and *Q*). *S–V*: Immunohistochemistry for IαI in normal (*S* and *T*) and T1D (*U* and *V*) tissues. *T* and *V*: Higher magnification of the boxed areas in *S* and *U*, respectively. *W*: Morphometric quantification of the PLN IαI-positive tissue area. Blue bar, normal tissues; red bar, diabetic tissues. Data are mean ± SD of the measurements obtained from tissues of 10 healthy and 8 T1D donors. *$P = 0.0015$ vs. normal tissues. *X–Â*: Immunohistochemistry for TSG-6 in normal (*X* and *Y*) and diabetic (*Z* and *Â*) tissues. *Y* and *Â*: Higher magnification of the boxed areas in *X* and *Z*, respectively. *Ã*: Morphometric quantification of the PLN TSG-6–positive tissue area. Blue bar, normal tissues; red bar, diabetic tissues. Data are mean ± SD of the measurements obtained from tissues of 10 healthy and 8 T1D donors. There was a trend of borderline significance toward reduced TSG-6 staining area in diabetic PLN ($P = 0.0728$). Images were prepared from nPOD cases 6196 (healthy) and 6052 (T1D). Scale bars: 100 μm (*S*, *U*, *X*, and *Z*) and 10 μm (*T*, *V*, *Y*, and *Â*). See also Supplementary Fig. 9.

release, it seems plausible that the same process may occur for TSG-6 in the islet.

The influence of HA and hyaladherin structural variations and binding properties on insulitis deserves further investigation. Alterations in islet ECM integrity may precede the initiation of inflammation as it has been described in other inflammatory conditions (40,52). Intravital imaging studies in a mouse diabetes model showed that β-cell killing was preceded by cytotoxic T-cell trapping within the vicinity of the β-cells at sites of capillary leakage (53). Cytotoxic T-cell arrest may result from altered ECM at these sites, recapitulating our in vitro observation that exposure of human monocytes and T cells to an HA- and a versican-rich ECM impedes their spreading and migration (22,47). Additionally, resistance to diabetes development was induced in the NOD mouse by blocking the HA receptor CD44, which supports HA involvement in disease pathogenesis (10). Increased quantity of HA and some hyaladherins in T1D islets indicates that alterations in the islet ECM are part of T1D pathogenesis. The importance of the role of HA and hyaladherins in islet inflammation and T1D will be better clarified using animal models.

Our third major finding is that of HA and hyaladherin increase in lymph nodes and spleens in specific regions of B- and T-cell activation in T1D. In lymphoid tissue, upon antigen encounter, the antigen-presenting cells initiate interactions with B and T cells that lead to antibody production, proliferation, and differentiation to memory or effector cells. These interactions and events take place in the well-defined B- and T-cell compartments that contain a reticular network, which we now show to be HA enriched. We have previously identified a role for HA in controlling T-cell movement and demonstrated that intact HA augments the suppressor activity and viability of regulatory T cells (6,22). HA production is known to induce dendritic cell phenotypic maturation, cytokine production, and antigen presentation (18,19,43,44,54). HA has also been localized to the immune synapse, suggesting a key role in antigen presentation and immune signaling (19,20,54). We show that HA deposits were concentrated within the follicular GC and T-cell areas, specialized regions of lymphatic tissues where B cells and T cells encounter their cognate antigens, and undergo differentiation and activation. It may be that HA in the follicular GCs and T-cell areas modulates immune cell interactions or their adhesive and migratory properties, promoting T-cell phenotype changes (55). However, the mechanisms by which altered HA affects these immune events remain to be determined.

The functional relevance of IαI accumulation and TSG-6 presence in lymphoid tissue in T1D is also largely unknown. In an in vitro system, IαI has been shown to be critical for T-cell adhesion to HA-rich matrices. TSG-6 is also known to inhibit the activation of both T cells and antigen-presenting cells in a CD44-dependent manner (49). Proteins that bind HA are necessary for promoting the organization of HA for optimal leukocyte adhesion and activation, indicating that the composition and organization of the ECM may be critical to determining lymphoid and myeloid phenotypes in lymph nodes and spleen.

Together, our observations suggest that events contributing to T1D may be taking place in tissues other than the pancreatic islets. The finding of specific changes in HA and associated proteins, not only in pancreatic islets but also in PLNs and spleen, raises the possibility that HA within these tissues in diabetic subjects may potentiate immune responses and contribute to failures in immune tolerance. It is tempting to speculate that altered HA-rich matrices in specific immune cell sites might thereby modulate antigen presentation, lymphocyte trafficking, or proliferation (55) in ways that lead to enhanced or sustained T-cell activation and loss of immune tolerance. Our finding of increases in HA and specific hyaladherins in islets and lymphoid tissues in T1D raises important new questions regarding the functional significance of these specific ECM components in the pathogenesis of TID and suggest possible new targets in the treatment of this disease.

Acknowledgments. The authors thank Cara Appel, research scientist and imaging specialist at the Histology and Imaging Core, University of Washington Medicine at South Lake Union (Seattle, WA), for assistance with the morphometric quantification. The authors also thank Virginia M. Green of the Matrix Biology Program, Benaroya Research Institute, for careful editing and preparation of the manuscript. The authors acknowledge the investigators and staff of Translational Research at the Benaroya Research Institute for subject recruitment, as well as the Clinical Core Laboratory for sample processing and handling.

Funding. This research was performed with the support of the Network for Pancreatic Organ Donors with Diabetes (nPOD), a collaborative type 1 diabetes research project sponsored by JDRF. This study was supported by U01-AI-101984 (to P.L.B. and T.N.W.), R01-DK-096087 and R01-HL-113294 (to P.L.B.), JDRF nPOD grant 25-2010-648 (to T.N.W.), R01-AR-03729 (BIRT Supplement to T.N.W.), and the Cooperative Study Group for Autoimmune Disease Prevention Innovative Project (under AI-101984 to T.N.W.). National Institutes of Health National Institute of Diabetes and Digestive and Kidney Diseases grant P30-DK-17047 provided core support.

Duality of Interest. No potential conflicts of interest relevant to this article were reported.

Author Contributions. M.B. contributed to the study design; performance of the experiments; data research and analysis; and writing, review, and editing of the manuscript. P.Y.J. contributed to the performance of the experiments using immunohistochemistry. S.P.-P. contributed to the experimental design and discussion. N.N. contributed to performing the serum HA assays. A.J.D. contributed reagents and to the discussion. P.L.B. contributed to the writing, review, and editing of the manuscript. T.N.W. contributed to the research design and writing, review, and editing of the manuscript. T.N.W. is the guarantor of this work and, as such, had full access to all the data in the study and takes responsibility for the integrity of the data and the accuracy of the data analysis.

Prior Presentation. Parts of this study were presented orally at the Network for Pancreatic Organ Donors with Diabetes (nPOD) 5th Annual Meeting, Atlantic Beach, FL, 10–13 February 2013, and as a poster at the International Society for Hyaluronan Sciences Meeting, Oklahoma City, OK, 2–7 June 2013.

References

1. Atkinson MA, Gianani R. The pancreas in human type 1 diabetes: providing new answers to age-old questions. Curr Opin Endocrinol Diabetes Obes 2009;16:279–285
2. Eizirik DL, Colli ML, Ortis F. The role of inflammation in insulitis and beta-cell loss in type 1 diabetes. Nat Rev Endocrinol 2009;5:219–226
3. Parnaud G, Hammar E, Ribaux P, Donath MY, Berney T, Halban PA. Signaling pathways implicated in the stimulation of beta-cell proliferation by extracellular matrix. Mol Endocrinol 2009;23:1264–1271
4. Kaido T, Yebra M, Cirulli V, Rhodes C, Diaferia G, Montgomery AM. Impact of defined matrix interactions on insulin production by cultured human beta-cells: effect on insulin content, secretion, and gene transcription. Diabetes 2006;55:2723–2729
5. Wang RN, Rosenberg L. Maintenance of beta-cell function and survival following islet isolation requires re-establishment of the islet-matrix relationship. J Endocrinol 1999;163:181–190
6. Bollyky PL, Bogdani M, Bollyky JB, Hull RL, Wight TN. The role of hyaluronan and the extracellular matrix in islet inflammation and immune regulation. Curr Diab Rep 2012;12:471–480
7. Korpos E, Kadri N, Kappelhoff R, et al. The peri-islet basement membrane, a barrier to infiltrating leukocytes in type 1 diabetes in mouse and human. Diabetes 2013;62:531–542
8. Hammar E, Parnaud G, Bosco D, et al. Extracellular matrix protects pancreatic beta-cells against apoptosis: role of short- and long-term signaling pathways. Diabetes 2004;53:2034–2041
9. Irving-Rodgers HF, Ziolkowski AF, Parish CR, et al. Molecular composition of the peri-islet basement membrane in NOD mice: a barrier against destructive insulitis. Diabetologia 2008;51:1680–1688
10. Weiss L, Slavin S, Reich S, et al. Induction of resistance to diabetes in non-obese diabetic mice by targeting CD44 with a specific monoclonal antibody. Proc Natl Acad Sci U S A 2000;97:285–290
11. Ziolkowski AF, Popp SK, Freeman C, Parish CR, Simeonovic CJ. Heparan sulfate and heparanase play key roles in mouse β cell survival and autoimmune diabetes. J Clin Invest 2012;122:132–141
12. Kvezereli M, Michie SA, Yu T, Creusot RJ, Fontaine MJ. TSG-6 protein expression in the pancreatic islets of NOD mice. J Mol Histol 2008;39:585–593
13. Day AJ, Prestwich GD. Hyaluronan-binding proteins: tying up the giant. J Biol Chem 2002;277:4585–4588
14. Laurent TC, Laurent UB, Fraser JR. The structure and function of hyaluronan: an overview. Immunol Cell Biol 1996;74:A1–A7
15. Day AJ, de la Motte CA. Hyaluronan cross-linking: a protective mechanism in inflammation? Trends Immunol 2005;26:637–643
16. Jiang D, Liang J, Noble PW. Hyaluronan as an immune regulator in human diseases. Physiol Rev 2011;91:221–264
17. Termeer C, Benedix F, Sleeman J, et al. Oligosaccharides of hyaluronan activate dendritic cells via toll-like receptor 4. J Exp Med 2002;195:99–111
18. Mummert ME, Mummert D, Edelbaum D, Hui F, Matsue H, Takashima A. Synthesis and surface expression of hyaluronan by dendritic cells and its potential role in antigen presentation. J Immunol 2002;169:4322–4331
19. Bollyky P, Evanko S, Wu R, et al. Th1 cytokines promote T-cell binding to antigen-presenting cells via enhanced hyaluronan production and accumulation at the immune synapse. Cell Mol Immunol 2010;7:211–220
20. Bollyky PL, Lord JD, Masewicz SA, et al. Cutting edge: high molecular weight hyaluronan promotes the suppressive effects of CD4+CD25+ regulatory T cells. J Immunol 2007;179:744–747
21. Bollyky PL, Falk BA, Wu RP, Buckner JH, Wight TN, Nepom GT. Intact extracellular matrix and the maintenance of immune tolerance: high molecular weight hyaluronan promotes persistence of induced CD4+CD25+ regulatory T cells. J Leukoc Biol 2009;86:567–572
22. Evanko SP, Potter-Perigo S, Bollyky PL, Nepom GT, Wight TN. Hyaluronan and versican in the control of human T-lymphocyte adhesion and migration. Matrix Biol 2012;31:90–100
23. Hull RL, Johnson PY, Braun KR, Day AJ, Wight TN. Hyaluronan and hyaluronan binding proteins are normal components of mouse pancreatic islets and are differentially expressed by islet endocrine cell types. J Histochem Cytochem 2012;60:749–760
24. Fujimoto T, Savani RC, Watari M, Day AJ, Strauss JF 3rd. Induction of the hyaluronic acid-binding protein, tumor necrosis factor-stimulated gene-6, in cervical smooth muscle cells by tumor necrosis factor-alpha and prostaglandin E(2). Am J Pathol 2002;160:1495–1502
25. Baranova NS, Foulcer SJ, Briggs DC, et al. Inter-α-inhibitor impairs TSG-6-induced hyaluronan cross-linking. J Biol Chem 2013;288:29642–29653
26. Rountree AM, Reed BJ, Cummings BP, et al. Loss of coupling between calcium influx, energy consumption and insulin secretion associated with development of hyperglycaemia in the UCD-T2DM rat model of type 2 diabetes. Diabetologia 2013;56:803–813
27. Bock T, Svenstrup K, Pakkenberg B, Buschard K. Unbiased estimation of total beta-cell number and mean beta-cell volume in rodent pancreas. APMIS 1999;107:791–799
28. Bonner-Weir S, Orci L. New perspectives on the microvasculature of the islets of Langerhans in the rat. Diabetes 1982;31:883–889
29. Brissova M, Fowler MJ, Nicholson WE, et al. Assessment of human pancreatic islet architecture and composition by laser scanning confocal microscopy. J Histochem Cytochem 2005;53:1087–1097
30. Bosco D, Armanet M, Morel P, et al. Unique arrangement of alpha- and beta-cells in human islets of Langerhans. Diabetes 2010;59:1202–1210
31. Henderson JR, Moss MC. A morphometric study of the endocrine and exocrine capillaries of the pancreas. Q J Exp Physiol 1985;70:347–356
32. van Krieken JH, te Velde J. Normal histology of the human spleen. Am J Surg Pathol 1988;12:777–785
33. Willard-Mack CL. Normal structure, function, and histology of lymph nodes. Toxicol Pathol 2006;34:409–424
34. Willcox A, Richardson SJ, Bone AJ, Foulis AK, Morgan NG. Analysis of islet inflammation in human type 1 diabetes. Clin Exp Immunol 2009;155:173–181
35. Kaldjian EP, Gretz JE, Anderson AO, Shi Y, Shaw S. Spatial and molecular organization of lymph node T cell cortex: a labyrinthine cavity bounded by an epithelium-like monolayer of fibroblastic reticular cells anchored to basement membrane-like extracellular matrix. Int Immunol 2001;13:1243–1253
36. Nieuwdorp M, Mooij HL, Kroon J, et al. Endothelial glycocalyx damage coincides with microalbuminuria in type 1 diabetes. Diabetes 2006;55:1127–1132
37. Van Deijnen JH, Van Suylichem PT, Wolters GH, Van Schilfgaarde R. Distribution of collagens type I, type III and type V in the pancreas of rat, dog, pig and man. Cell Tissue Res 1994;277:115–121
38. Otonkoski T, Banerjee M, Korsgren O, Thornell LE, Virtanen I. Unique basement membrane structure of human pancreatic islets: implications for beta-cell growth and differentiation. Diabetes Obes Metab 2008;10(Suppl. 4):119–127
39. Wang A, de la Motte C, Lauer M, Hascall V. Hyaluronan matrices in pathobiological processes. FEBS J 2011;278:1412–1418
40. de la Motte CA. Hyaluronan in intestinal homeostasis and inflammation: implications for fibrosis. Am J Physiol Gastrointest Liver Physiol 2011;301:G945–G949
41. Winkler CW, Foster SC, Itakura A, et al. Hyaluronan oligosaccharides perturb lymphocyte slow rolling on brain vascular endothelial cells: implications for inflammatory demyelinating disease. Matrix Biol 2013;32:160–168
42. Termeer C, Sleeman JP, Simon JC. Hyaluronan—magic glue for the regulation of the immune response? Trends Immunol 2003;24:112–114
43. Mummert ME. Immunologic roles of hyaluronan. Immunol Res 2005;31:189–206
44. Galandrini R, Galluzzo E, Albi N, Grossi CE, Velardi A. Hyaluronate is co-stimulatory for human T cell effector functions and binds to CD44 on activated T cells. J Immunol 1994;153:21–31

45. Chang MY, Chan CK, Braun KR, et al. Monocyte-to-macrophage differentiation: synthesis and secretion of a complex extracellular matrix. J Biol Chem 2012;287:14122–14135
46. Baranova NS, Nilebäck E, Haller FM, et al. The inflammation-associated protein TSG-6 cross-links hyaluronan via hyaluronan-induced TSG-6 oligomers. J Biol Chem 2011;286:25675–25686
47. Potter-Perigo S, Johnson PY, Evanko SP, et al. Polyinosine-polycytidylic acid stimulates versican accumulation in the extracellular matrix promoting monocyte adhesion. Am J Respir Cell Mol Biol 2010;43:109–120
48. Lesley J, Gál I, Mahoney DJ, et al. TSG-6 modulates the interaction between hyaluronan and cell surface CD44. J Biol Chem 2004;279:25745–25754
49. Kota DJ, Wiggins LL, Yoon N, Lee RH. TSG-6 produced by hMSCs delays the onset of autoimmune diabetes by suppressing Th1 development and enhancing tolerogenicity. Diabetes 2013;62:2048–2058
50. Maina V, Cotena A, Doni A, et al. Coregulation in human leukocytes of the long pentraxin PTX3 and TSG-6. J Leukoc Biol 2009;86:123–132
51. Nagyeri G, Radacs M, Ghassemi-Nejad S, et al. TSG-6 protein, a negative regulator of inflammatory arthritis, forms a ternary complex with murine mast cell tryptases and heparin. J Biol Chem 2011;286:23559–23569
52. Spenlé C, Hussenet T, Lacroute J, et al. Dysregulation of laminins in intestinal inflammation. Pathol Biol (Paris) 2012;60:41–47
53. Coppieters K, Amirian N, von Herrath M. Intravital imaging of CTLs killing islet cells in diabetic mice. J Clin Invest 2012;122:119–131
54. Mummert ME, Mohamadzadeh M, Mummert DI, Mizumoto N, Takashima A. Development of a peptide inhibitor of hyaluronan-mediated leukocyte trafficking. J Exp Med 2000;192:769–779
55. Bajénoff M, Egen JG, Koo LY, et al. Stromal cell networks regulate lymphocyte entry, migration, and territoriality in lymph nodes. Immunity 2006;25:989–1001